Research Square

Preprints are preliminary reports that have not undergone peer review.
They should not be considered conclusive, used to inform clinical practice,
or referenced by the media as validated information.

# Non-equilibrium crystallisation of aqueous sol-gel-derived $Bi_4Ti_3O_{12}$ thin films using concentrated solar energy

**Carlos Gumiel**

cgumiel@nebrija.es

Universidad Nebrija

**María Colado**

Universidad Nebrija

**Daniel Gomez-Lendinez**

Universidad Nebrija

**Antonio Cañadilla**

University of Castilla-La Mancha

**Ana Romero**

University of Castilla-La Mancha

**Gloria Patricia Rodríguez**

University of Castilla-La Mancha

**Amador Caballero**

Instituto de Cerámica y Vidrio

**Rafael Barea**

Universidad Nebrija

**Marco Peiteado**

Instituto de Cerámica y Vidrio

**Teresa Jardiel**

Instituto de Cerámica y Vidrio

**Research Article**

**Keywords:** Concentrated solar energy, BIT thin films, Aqueous sol-gel, Microstructural control, Rapid thermal annealing

**Posted Date:** November 2nd, 2026

**DOI:** https://doi.org/10.21203/rs.3.rs-11307104/v1

**License:** This work is licensed under a Creative Commons Attribution 4.0 International License.
Read Full License

**Additional Declarations:** No competing interests reported.

# Non-equilibrium crystallisation of aqueous sol-gel-derived $Bi_4Ti_3O_{12}$ thin films using concentrated solar energy

C. Gumiel[a*], M. Colado[a], D. Gomez-Lendinez[a], A. Cañadilla[b], A. Romero[b], G. P. Rodríguez[c], A.C. Caballero[d], R. Barea[a], M. Peiteado[d], T. Jardiel[d*]

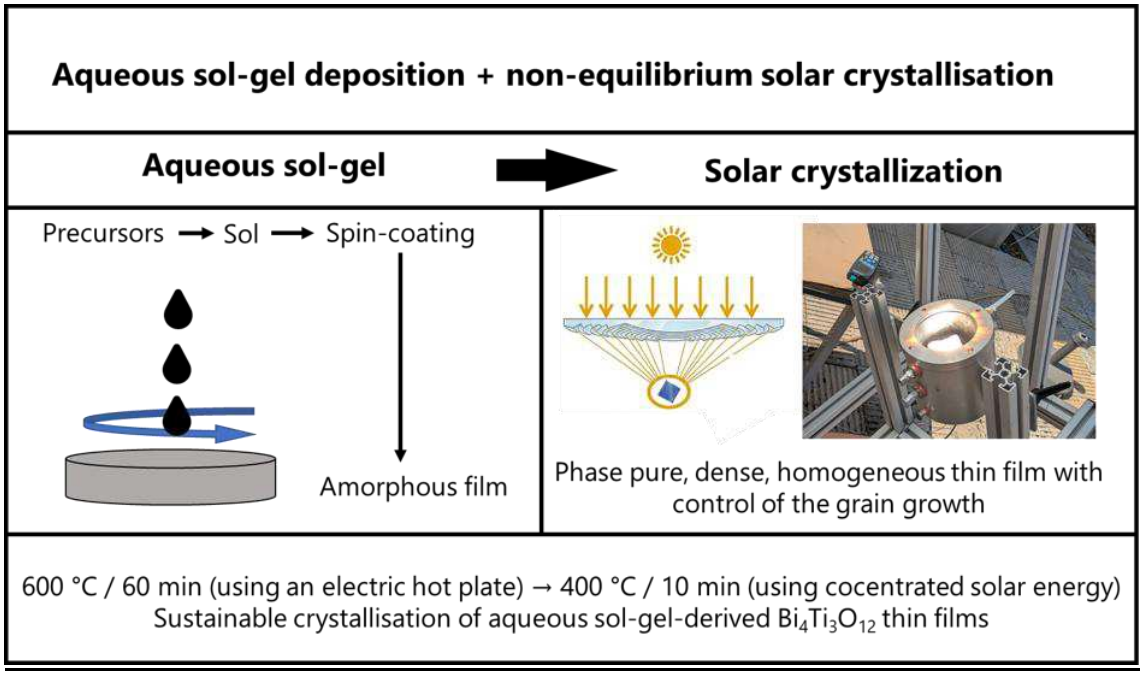
a. Department of Industrial Engineering, Universidad Nebrija, Campus Madrid-Princesa, 28015 Madrid, Spain
b. School of Industrial and Aerospace Engineering, University of Castilla-La Mancha (EIIAA-UCLM), 45071 Toledo, Spain
c. Higher Technical School of Industrial Engineering, Ciudad Real, University of Castilla-La Mancha (ETSII-UCLM), Spain
d. Department of Electroceramics, Instituto de Cerámica y Vidrio (CSIC), Madrid 28049, Spain

*Corresponding author: C. Gumiel, E-mail address: cgumiel@nebrija.es
*Corresponding author: T. Jardiel, E-mail address: jardiel@icv.csic.es

**Abstract**

Controlling the crystallisation of sol-gel-derived oxide thin films remains one of the most critical challenges in chemical solution deposition, as the post-deposition thermal treatment largely determines phase formation, densification and microstructural development. This issue is particularly relevant for layered ferroelectric oxides such as $Bi_4Ti_3O_{12}$ (BiT), whose crystallisation under conventional thermal conditions often promotes exaggerated anisotropic grain growth and the formation of secondary phases associated with bismuth volatilisation. In this work, $Bi_4Ti_3O_{12}$ thin films were prepared by an aqueous sol-gel route combined with spin coating and subsequently crystallised using concentrated solar energy (CSE) as an alternative radiative annealing strategy. The use of an aqueous precursor chemistry avoids organic solvents, while the high radiative fluxes delivered by a Fresnel-lens-based solar concentrator provide access to thermal conditions far from equilibrium. The crystallisation behaviour and microstructural evolution of the films were systematically compared with those obtained by conventional hot-plate annealing. The results demonstrate that concentrated solar irradiation fundamentally modifies the crystallisation pathway of the sol-gel-derived films. Whereas excessive radiative input accelerates anisotropic grain growth and promotes pyrochlore formation, a narrow processing window centred around 400 °C and short dwell times enables complete phase formation, good densification and microstructural homogeneity while suppressing the equilibrium growth of plate-like grains. The study further reveals that the combination of rapid heating rates and strong thermal gradients allows the balance between crystallisation, densification and grain growth to be finely controlled. These findings demonstrate that concentrated solar energy represents a powerful processing tool for tailoring the crystallisation of sol-gel-derived oxide thin films under non-equilibrium conditions. Together with the significant reduction in processing temperature and thermal treatment time, this approach offers a sustainable and energy-efficient alternative for the thermal processing of functional oxide coatings.

**Graphical Abstract**




**Keywords:** Concentrated solar energy; BIT thin films; Aqueous sol-gel; Microstructural control; Rapid thermal annealing

**Highlights:**

- Concentrated solar energy modifies the crystallisation pathway of aqueous sol-gel derived $Bi_4Ti_3O_{12}$ thin films.
- An alternative sintering method using renewable energy source.
- An operational window near 400 °C produces homogeneous films with complete phase formation.
- Solar annealing reduces processing temperature and time compared with conventional heating.

## 1. Introduction

The development of advanced functional materials in the form of thin-films is central to a wide range of modern high-tech applications, enabling device miniaturisation while substantially improving performance. Thin films are essential components in microelectronics, sensors, energy-related devices, optoelectronics or photocatalytic systems, where functionality depends largely on achieving precise control of the film's microstructure [1-4]. Nevertheless, thin film processing remains a challenge. In conventional industrial processing, sophisticated physical and chemical vapour deposition techniques (sputtering, CVD, ALD) are generally used, offering an appropriate control over the composition, thickness, and uniformity of the films, albeit at the cost of a high energy consumption [5-7]. In parallel, alternative wet-chemistry based approaches such as sol-gel processing, chemical solution deposition, and related routines, have been explored due to their compositional flexibility, scalability and potential for reducing the energy (and economic) costs [8-10]. Regardless of the deposition method, both vapour-phase and solution-based techniques usually produce films that are amorphous or poorly crystallized in the as-deposited state, so post-deposition heat treatments are required to induce crystallization, densification and phase formation. The thermal treatment therefore represents a critical step common to all deposition strategies and ultimately determines the final microstructure and functional response of the films. The most practical option involves completing the post-deposition annealing in furnace-based systems, where heat transfer is governed

primarily by conduction and convection within a spatially homogeneous temperature field. This entails high processing temperatures and long dwell times which, while promoting crystallization and densification, can also induce an excessive grain growth that typically brings detrimental effects. This is the case with layered oxide ceramics such as $Bi_4Ti_3O_{12}$ (BiT), a ferroelectric material attracting growing interest as a sustainable, lead-free alternative for electronic applications, including non-volatile ferroelectric memories and piezoelectric sensors. Under equilibrium conditions, the Aurivillius-type crystal structure of this oxide promotes grain growth in the a-b plane and eventually yields a strongly anisotropic microstructure composed of elongated plate-shaped grains [11]. An exaggerated growth of those grains can increase leakage currents and, because the (spontaneous) polarization of BiT is mainly confined to the a-b plane, it often impairs the ferroelectric switching. The situation is even more defiant when BiT is grown as a thin film on a substrate. During the mentioned post-deposition thermal treatment, the amorphous and/or partially reacted precursor undergoes rapid diffusion and nucleation directly on the substrate surface and, owing to the small film thickness and short diffusion distances, densification and grain growth occur simultaneously with phase formation [12,13]. This typically results in dense, well-adhered films, but with a pronounced overgrowth of the plate-shaped grains. In addition, the high surface-to-volume ratio characteristic of the film geometry gives rise to undesirable stoichiometric deviations associated with uncontrolled volatilisation of bismuth [14], further compromising the piezoelectric performance of the material. A common practice to avoid these issues involves doping BiT films with selected dopants, although this entails revisiting the entire deposition procedure to clearly determine how the incorporated species affect the microstructure and final properties of the resulting material. In contrast, without introducing compositional changes, a feasible strategy for modulating microstructural anisotropy and grain growth while preserving film densification is the so-called rapid thermal processing (RTP). Leaning on the use of halogen or infrared lamps in which heating occurs predominantly through radiation, these treatments enable fast heating rates, so that the material reaches high temperatures in very short periods of time [15-17]. Such rapid access to elevated temperatures can enhance the kinetic control over crystallization. In anisotropic systems where thermodynamically favoured orientations often dominate under conventional annealing conditions, it may also help to mitigate anisotropy-related effects and suppress excessive grain growth. Even so, the rapid thermal approach still presents inherent limitations, and particularly in the case of BiT, control of anisotropy and grain growth remains challenging by RPT [18]. On one hand, RTP lamps emit within a fixed and relatively narrow spectral range which makes that their radiative coupling with complex oxide ceramics such as $Bi_4Ti_3O_{12}$ may not be effective, mainly because the absorption characteristics of ceramics are wavelength-dependent and can even evolve during phase formation and densification [19,20]. But moreover, same as in conventional furnaces, lamp-based RTP systems are designed to ensure spatially homogeneous temperature fields, eventually promoting near-equilibrium thermal conditions despite the high heating rates [21]. The processing pathway of BiT however demands additional degrees of freedom, i.e. non-equilibrium kinetics scenarios to modulate the (thermodynamically driven) grain growth and microstructure development, especially in thin-film architectures.

In this context, the use of concentrated solar energy (CSE) emerges as an attractive alternative to be tested in the thermal processing of BiT thin films, as it offers a different approach to energy delivery and heat-matter interaction. As in lamp-based RTP systems, solar sintering relies on radiative heat transfer, but the nature of the radiation source and the resulting thermal regime are fundamentally different [22,23].

A first advantage lies in the spectral characteristics of the heat source. Concentrated solar radiation spans a broad wavelength range, from the ultraviolet to the near-infrared, which can promote more efficient and direct energy absorption within the thin film itself, thereby enabling faster and more selective heating of the active material [24]. Moreover, contrary to conventional processes where the higher the temperature needed, the higher the energy consumption, the costs of material processing using CSE are not dependent on the temperature [25]. It also provides substantially higher radiative fluxes: concentrated solar energy systems employ optical elements such as parabolic concentrators or Fresnel lenses to focus solar radiation onto a confined area, reaching power densities that can significantly exceed those of conventional furnace and lamp-based RTP systems [26,27]. This circumstance allows for ultra-fast heating rates, pronounced thermal gradients and intrinsically non-equilibrium thermal conditions which can strongly influence crystallisation kinetics and microstructural evolution. In anisotropic systems such as BiT that are

particularly sensitive to thermal history, these conditions can be especially advantageous, as they may allow densification to be decoupled from (excessive) grain growth. Finally, the use of solar radiation offers additional benefits beyond explicit microstructural control. The extremely high heating and cooling rates can significantly reduce overall processing times, thereby limiting secondary diffusion processes or unwanted interfacial reactions with substrates. And from a sustainability perspective, solar sintering involves using a renewable energy input, hence reducing the carbon footprint and energy consumption associated to high-temperature processing [26,28]. If solar concentration is carried out using a Fresnel lens, other positive aspects must also be considered. Facility and installation costs are very low, and overall costs are kept low independently of temperatures or time parameters, which makes the use of this kind of lens highly attractive for implementation in materials processing or microstructural and surface modifications [29].

In light of the above considerations, this work investigates the potential of concentrated solar energy (CSE) as an alternative thermal treatment for the crystallization and sintering of $Bi_4Ti_3O_{12}$ thin films. The objective is not simply to employ CSE as another (sustainable) heat source, but to exploit it as a processing tool capable of driving the system far from equilibrium, thereby enabling access to transient kinetic regimes in which densification and anisotropic grain growth can be partially decoupled. A Fresnel-lens solar concentrating system capable of achieving concentration ratios of up to 2644 suns (equivalent to approximately 264 W/cm² at an incident solar irradiance of 1 kW/m²) was used [30]. In order to clearly assess the effect of the non-equilibrium CSE thermal conditions on the microstructural evolution of the films, a comparative study is conducted with samples subjected to a conventional hot-plate thermal treatment.

## 2. Materials and methods

### 2.1 Experimental procedure

In order to ensure overall process sustainability, the $Bi_4Ti_3O_{12}$ films were prepared following an aqueous sol-gel deposition methodology, which while offering good compositional control, also avoids the use of energy-intensive vacuum techniques [31]. The production of the films comprises a first stage of obtaining the precursor solution and a second stage in which this is deposited on a substrate by spin coating. In a typical procedure, monometal solutions of $Bi^{3+}$ and $Ti^{4+}$ in aqueous medium are prepared individually and then mixed in stoichiometric proportions to generate a 0.2 M multimetal precursor solution [32]. Bismuth (III) citrate ($Bi(C_6H_5O_7)_3$, 99.99%, Aldrich) and titanium (IV) isopropoxide ($Ti(iOPr)_4$, 98+%, Acros) were used as metal precursors in a process that also involves ammonia, ethanolamine, citric acid, and hydrogen peroxide as pertinent additives to ensure stable solutions with appropriate rheology for the subsequent deposition process [33]. This was carried out in a spin coating machine (Laurel tech) using 1 cm² square $Pt(111)/Ti/SiO_2/Si$ substrates, whose surface was pre-treated to ensure a strong hydrophilic character. As for deposition, three drops of the multi-metal precursor solution are poured onto the rotating substrate (3000 rpm) and, after 30 seconds spinning, the deposited sample undergoes three consecutive stages of rapid drying at 95 °C, 200 °C, and 520 °C (1 min each) to remove the solvent and various processing additives [32]. The entire process is repeated eight times to eventually yield an 8-layered film that is still amorphous at this stage of the process.

The thermal annealing to crystallize the thin films was next conducted using the two aforementioned strategies: conventional heating on a hot plate and exposure to concentrated solar radiation. In the first case, the samples were placed directly on the preheated surface of the plate, Figures 1a and 1b, and subjected to consolidation temperatures up to 800 °C. On the other hand, the CSE system consisted of low-cost solar installation with a Fresnel lens attached to a Microtest ESS solar tracker, as depicted in Figures 1c-1e. The circular lens is made of acrylic material with a faceted surface, has a diameter of 900 mm and a central thickness of 3.17 mm, and exhibits a maximum concentration factor of 2644 (ratio of focal spot irradiance to incident irradiance) at a focal distance of 757 mm and a focal area of approximately 16 mm in diameter [30]. The lens is mounted on an aluminium support equipped with a rotor and a tilting mechanism to continuously track the sun's motion, and incorporates a shutter to regulate the amount of solar radiation

being transmitted to the Fresnel lens. This is a key factor to control the heating and working temperatures during the solar thermal treatment, achieving and maintaining the target sintering temperature. After passing through the lens, the concentrated solar radiation spot incises on the upper surface of the sample, positioned at the center of a reaction chamber. The sample is supported on an alumina holder coupled to a thermocouple, Figure 1f, and the temperature is monitored using a YCT-model YC-727D digital thermometer. As with hotplate annealing, various sintering temperatures and dwell times were investigated using the CSE setup. Figure 2 shows a representative thermogram of a solar sintering treatment carried out at 600 °C for 10 minutes, showing temperature fluctuations of just ±1 °C.

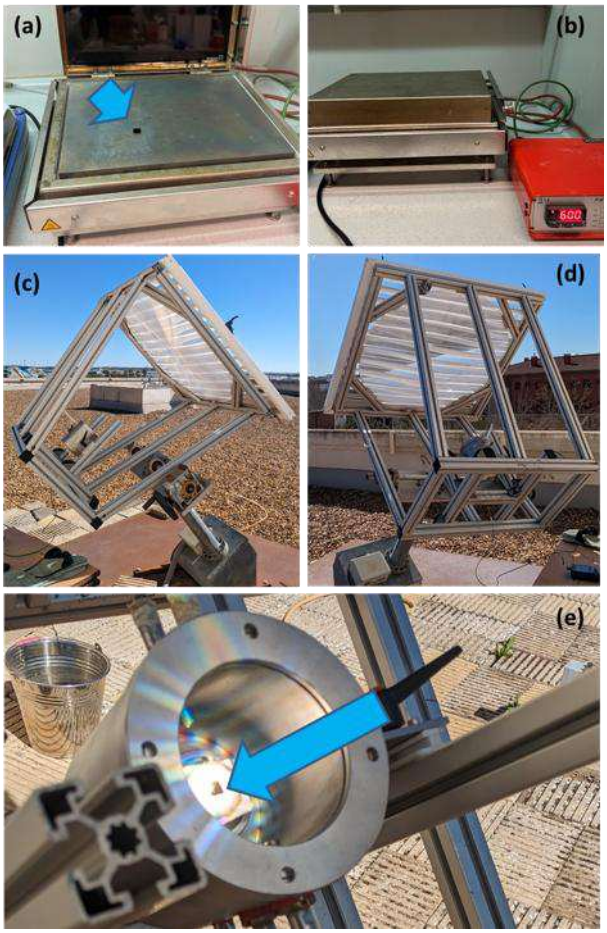



Figure 1. (a) BiT thin film sample (highlighted with a blue arrow) as placed on a pre-heated hot plate. (b) Hot plate lid closed during sintering at 600 °C during 1 hour. (c) Solar installation with a Fresnel Lens. (d) Shutter of the solar installation placed in front of the lens that solar radiation pass through. (e) Reaction chamber where the sample is placed (highlighted with a blue arrow).

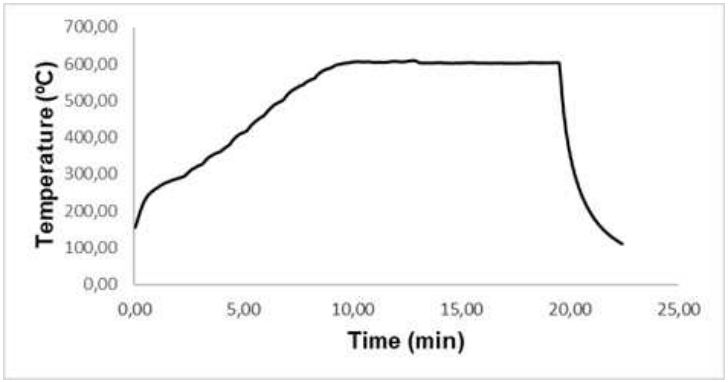



Figure 2. Thermogram corresponding to the film sintered at 600 °C for 10 minutes under concentrated solar energy.

### 2.2 Characterization techniques

The concentration of the monometallic precursor solutions was quantified by ICP-AES using a PerkinElmer Optima 3000 instrument. Crystalline phase identification of the deposited films was carried out by X-ray diffraction (XRD) using a Bruker D8 Advance diffractometer equipped with Cu Kα radiation. Microstructural investigations were performed by field-emission scanning electron microscopy (FESEM) with a Hitachi S-4700 cold FESEM microscope. Images were acquired predominantly in secondary electron mode, as backscattered electron observations did not reveal appreciable phase contrast. Additionally, selected films were chemically etched in diluted HCl solution prior to FESEM examination to enhance microstructural assessment.

## 3. Results and discussion

In order to establish a reference point for analysing the sintering conditions of $Bi_4Ti_3O_{12}$ thin films under solar radiation, their sintering behaviour on hot plates was first investigated. When a thin film deposited on a substrate is heated using a hot plate, heat transfer initially occurs through both conduction and radiation. However, according to Stefan-Boltzmann's law, the intensity of thermal radiation depends largely on the absolute temperature; hence, when relatively low temperatures are applied at the hot plate, the radiative component is negligible and the temperature increase of the film is governed mainly by heat conduction through the substrate. This scenario is expected in the films produced by the aqueous solution deposition methodology used in this work. Owing to a finer particle size and improved compositional homogeneity, samples obtained by wet chemical procedures can densify at temperatures lower than those produced via solid-state conventional processing, which typically require calcination and sintering temperatures around 850-1000 °C (or higher) [34]. Moreover, in the thin-film geometry, the intrinsically high surface-to-volume ratio facilitates diffusion, allowing a further reduction in sintering temperature and dwell time. With this in mind, hot-plate treatments were conducted at temperatures ranging from 400 to 800 °C, thereby relying primarily on a substrate-mediated heat-transfer mechanism. Figure 3 presents the corresponding XRD diffractograms, with the left panel showing samples tested with a dwell time of 30 minutes and the right panel those with a 60-minute plateau.

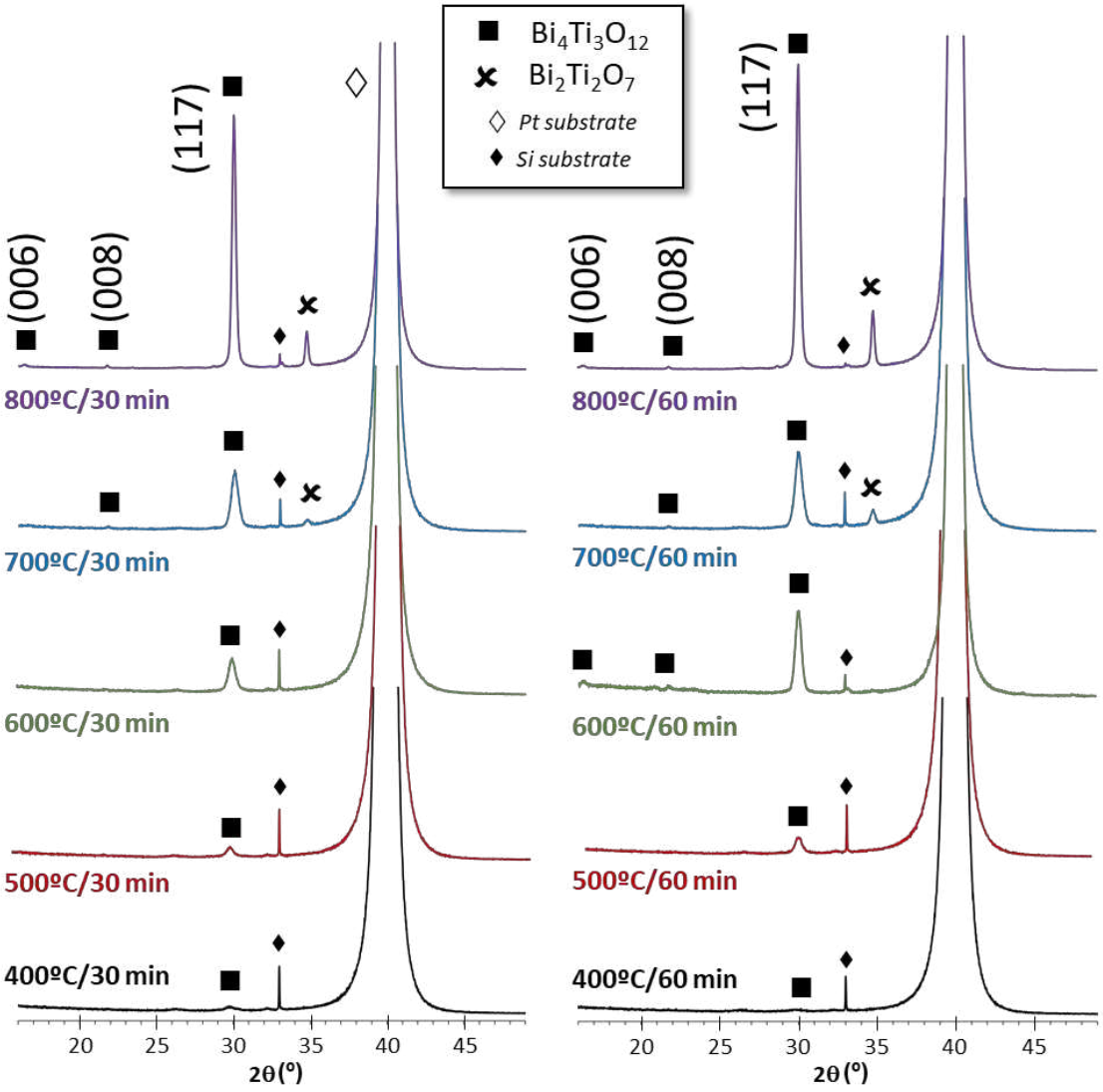



Figure 3. X-ray diffraction patterns of BiT thin films sintered on a hot-plate at temperatures ranging from 400 °C to 800 °C. Left: films treated with a dwell time of 30 minutes. Right: same tests with a sintering plateau of 60 minutes.

As depicted, in addition to strong reflections from the substrate (Si and Pt signals), several diffraction maxima can be indexed corresponding to the orthorhombic structure of $Bi_4Ti_3O_{12}$ (ICDD file no. 00-035-0795), though their number and intensity vary with the applied thermal treatment. A first maximum attributable to BiT is detected in films sintered at 400 °C, specifically the one corresponding to the (117) crystallographic plane, which is the peak of highest intensity of the orthorhombic phase [35,36]. However, this signal is barely incipient and broad at this temperature, indicating low crystallinity. It becomes more noticeable with increased temperature, and is at 600 °C when it gains relevant intensity and sharpness. At this temperature, the applied dwell time also leads to significant crystallographic differences. Extending the sintering time at 600 °C to 60 minutes results in a slight reduction in the system's crystallinity, as evidenced by broader and less well-defined diffraction peaks than in the previous diffractograms. This is accompanied by the detection of two additional $Bi_4Ti_3O_{12}$ reflections corresponding to the (006) and (008) planes. Both are 00l harmonics of the basal (001) plane and are indicative of a preferential orientation along the c-axis; moreover, combined with the lower relative intensity of the (117) peak, their presence may also point to

the onset of pronounced growth of elongated grains. Overall, it suggests that already at 600 °C, an increase in sintering time promotes the inherent anisotropy of the Aurivillius structure, in line with the expected evolution of the system towards thermodynamic equilibrium.

Interestingly, this trend changes when the hot-plate temperature is increased to 700 °C. It should be noted that, in hot-plate experiments, the samples are placed directly onto a plate that is already preheated to the target temperature, resulting in a rapid energy input. Under these conditions, the diffractogram obtained after sintering at 700 °C for 30 minutes, suggest that the higher temperature initially suppresses the anisotropic growth, as the reflections associated with the c axis are almost suppressed relative to the (117) reflection, which again becomes dominate. However, this goes in hand with the emergence of a secondary phase, evidenced by a diffraction maximum at 34.75°, whose intensity will progressively increase with both increasing the dwell time (sample treated at 700 °C for 1 hour) and the tests temperature (samples at 800 °C). This new reflection is indexed to the $Bi_2Ti_2O_7$ pyrochlore-type phase (ICDD file no. 00-032-0118) and its formation during the thermal consolidation of the BiT thin films can be associated to local deviations from stoichiometry induced by bismuth volatilization during annealing [37]. This is actually a critical feature to take into account in the film geometry, whereby the high surface-to-volume ratio aggravates such Bi loss [38], locally reducing the Bi:Ti ratio and so favouring the stabilization of titanium-rich phases such as $Bi_2Ti_2O_7$ over the desired Aurivillius $Bi_4Ti_3O_{12}$ phase [39]. Therefore, based on the thermal sequence disclosed by the XRD investigations, the most suitable hot-plate treatment to consolidate the BiT thin films without inducing excessive grain growth nor generating secondary phases, is the one performed at 600 °C for 30 min. This scenario was next confirmed by FESEM analyses. The micrographs in Figure 4a, corresponding to the sample sintered at 600 °C for 30 minutes, reveal the formation of a relatively dense film with a uniform thickness of approximately 300 nm. The sintered BiT grains exhibit an irregular morphology, most clearly observed in the top-view image shown in Figure 4b, also indicating that the anisotropic growth has not yet developed. Similarly, no clear preferential growth was detected in the sample treated at 600 °C for 1 hour, despite the initial indications from XRD analyses.

On the contrary, as the processing temperature increases, the films begin to display noticeable signs of microstructural degradation. Figure 4c shows the film sintered at 700 °C for 30 minutes and reveals the presence of darker regions surrounded by bright, rounded edges. These features may result from the formation of a Bi-rich liquid phase followed by its subsequent volatilisation. The associated loss of stoichiometry is likely responsible for the formation of the $Bi_2Ti_2O_7$ pyrochlore phase detected by XRD (although direct confirmation by SEM-EDX is not feasible due to the compositional similarity to the $Bi_4Ti_3O_{12}$ phase and the nanometre-scale size of the grains). An even more heterogeneous microstructure, exhibiting further signs of decomposition, is observed in Figure 4d, which corresponds to the film treated at 800 °C for 1 hour. Under these conditions, volatilisation is more pronounced, and some degree of anisotropic growth (manifested by the incipient elongation of the grains) can also be discerned as a consequence of the higher energy input.

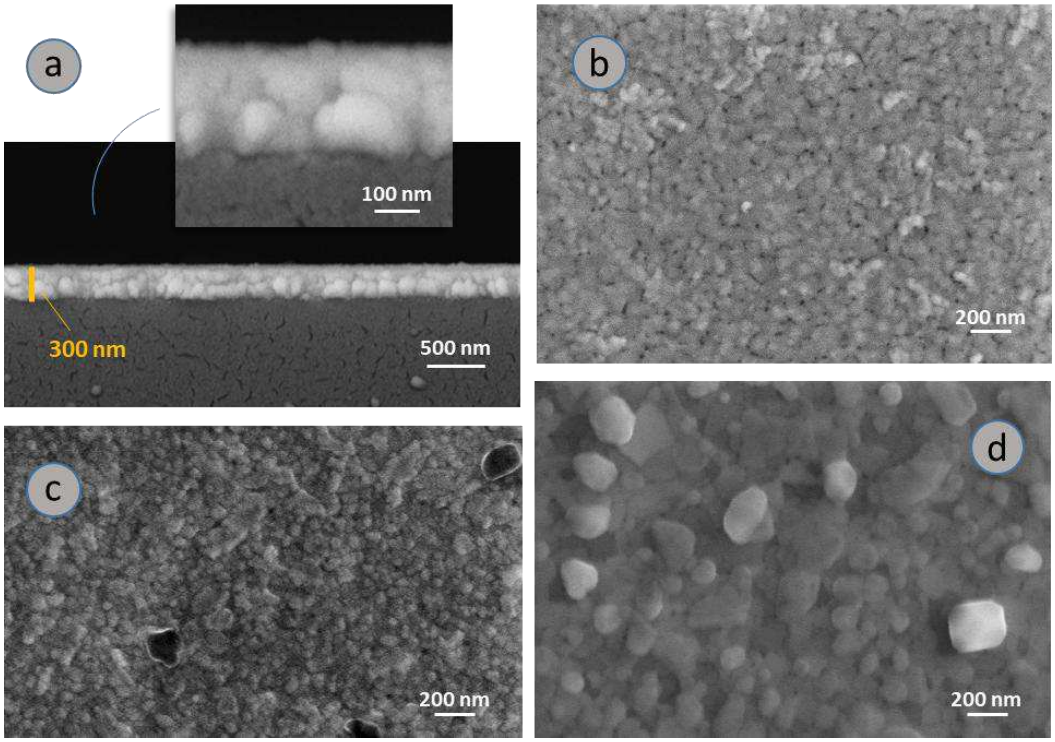



Figure 4. FESEM micrographs of the BiT thin films sintered on a hot plate. a) and b) film sintered at 600 °C for 30 minutes. c) Sample treated a 700 °C during 30 minutes. d) Film sintered 800 °C for 1 hour.

Following the hot-plate experiments, sintering studies under solar irradiation were initiated. As noted earlier, this approach entails a shift in the dominant heat transfer mechanism, from conduction to radiation. In addition, the Fresnel lens system concentrates the incident solar radiation onto a well-defined region, significantly increasing the local energy density delivered to the sample [30,40] (Figure 5 illustrates this effect, showing the groove left by the concentrated solar radiation on the sample). Therefore, unlike hot-plate annealing, where the system evolves under near-equilibrium thermal conditions, the highly localised and radiative nature of CSE processing introduces strong thermal gradients and ultra-fast heating rates that may fundamentally modify the crystallisation pathway and ultimately promote a non-equilibrium microstructural evolution.

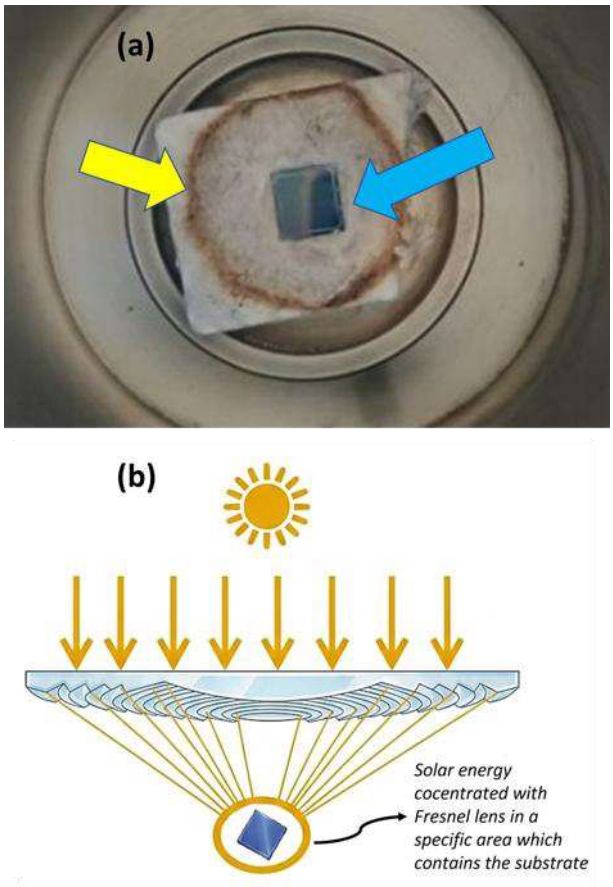



Figure 5. a) Location of the film sample inside the CSE chamber and the groove formed by the impingement of solar radiation. b) Schematic diagram illustrating how the Fresnel lens concentrates solar radiation onto the area where the sample is positioned.

On this basis, and considering the higher energy input, the first CSE tests were conducted at 600 °C with a reduced dwell time of just 5-10 minutes. It should be noted that the temperatures reported for all the CSE experiments correspond to measurements performed at the rear side of the samples. Due to the direct irradiation of the film surface by concentrated solar flux, the actual temperature at the irradiated film surface may be higher than the recorded value, leading to additional thermal gradients across the sample. Therefore, the observed differences between hot-plate and CSE treatments arise not only from the radiative nature of the heating process and the associated non-equilibrium conditions, but also potentially from differences between the measured and actual surface temperatures of the films.

The XRD diffractograms obtained from these two treatments are shown in Figure 6a and reveal some notable findings. On one hand, diffraction maxima corresponding to the orthorhombic phase of $Bi_4Ti_3O_{12}$ are again observed, but with higher intensities and narrower widths than in any of the hot-plate tests (nor even in those conducted at 800 °C). This observation confirms that crystallization is strongly enhanced under CSE conditions. Moreover, the predominance of 00l harmonic reflections, with two additional peaks indexed to the (0010) and (0014) planes, also suggests strong anisotropic growth of the BiT grains. On the other hand, a significant increase in the intensity of the diffraction maximum associated with the $Bi_2Ti_2O_7$ pyrochlore phase (around 35°) is also detected. As discussed above, this behaviour is attributed to compositional fluctuations caused by a bismuth volatilization, and may again indicate accelerated kinetics. These interpretations are supported by the corresponding FESEM characterization.

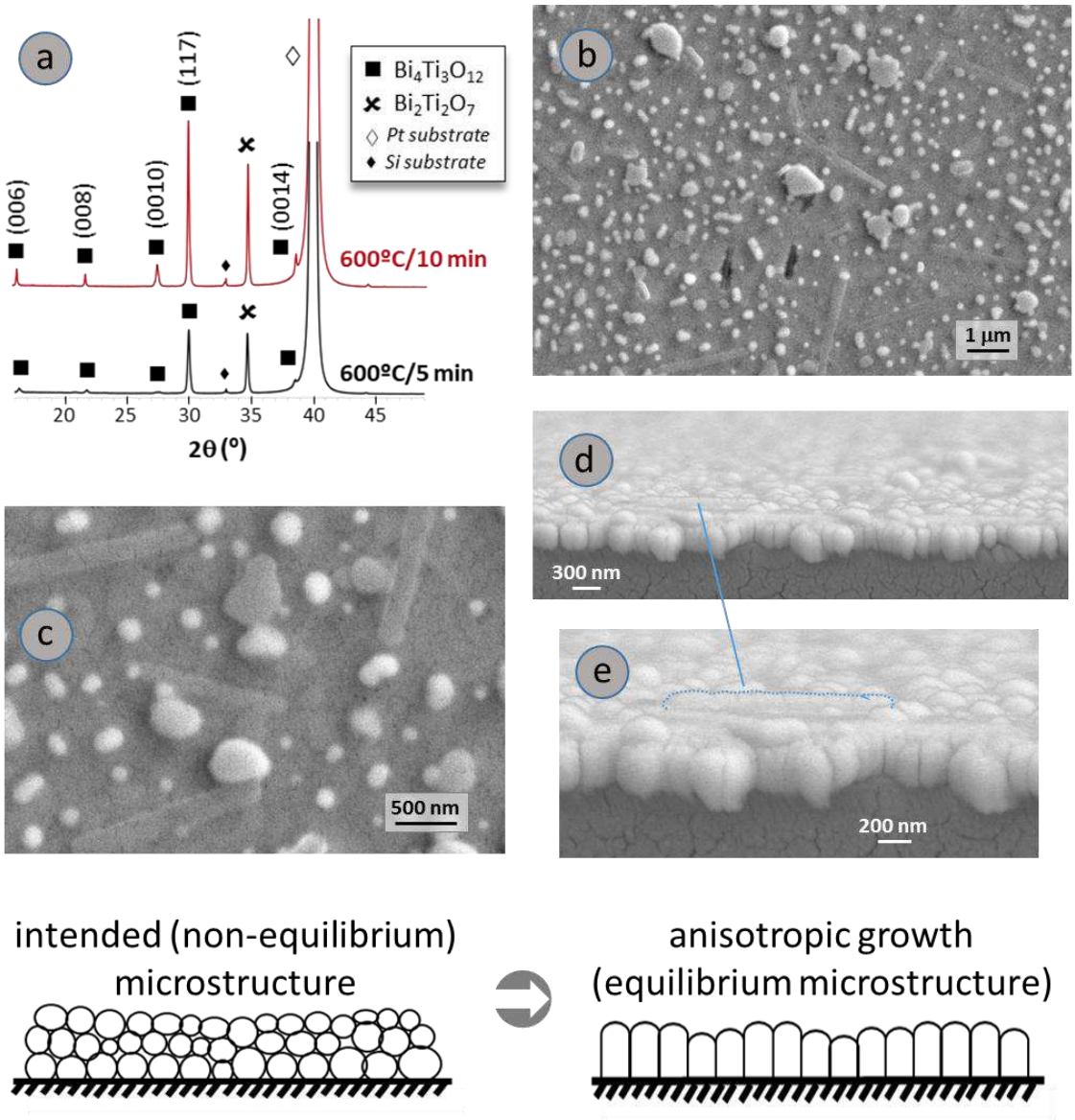



Figure 6. a) XRD patterns of BiT films sintered at 600 °C for 10 and 5 minutes under solar radiation (CSE). b-e) FESEM micrographs of the CSE film sintered at 600 °C for 10 minutes: b) top-view image, c) enlarged image of the plate-shaped crystallized grains, d) cross-sectional image showing the elongated growth of the BiT grains from the substrate and e) magnified image highlighting the presence of a large horizontal plate. The schematic diagram illustrates the differences between the intended (non-equilibrium) microstructure and the equilibrium configuration attained.

Figures 6b and 6c present top-view images of the film sintered at 600 °C for 10 minutes under concentrated solar radiation. As occurred with the high-temperature hot-plate experiments (Figures 4c and 4d), a highly reacted and poorly homogeneous microstructure is attained; however, some notable differences are evident. In addition to irregularly shaped features that may originate from a liquid-phase formation (followed by partial volatilisation), some grains now display exaggerated anisotropic growth. This leads to the crystallization of large platelets with lengths of up to 2 □m. Cross-sectional micrographs of this sample (Figures 6d and 6e) further show that, although the film thickness stays within the same ~300 nm range as in the hot-plate sintering tests, the BiT grains emerge from the substrate surface in the form of elongated, plate-like structures (providing also some space for the big platelets to grow parallel to the substrate, as

highlighted in Figure 6e). As discussed, this morphology corresponds to the equilibrium configuration of BiT and therefore indicates that, in the CSE-treated samples, a sintering temperature of 600 °C is too high to circumvent the structural anisotropy inherent to the system. Accordingly, further CSE-tests were carried out by progressively reducing the film sintering temperature (by adjusting the radiation transmitted through the lens shutter), while initially maintaining a fixed dwell time of 10 minutes. The corresponding XRD patterns are shown in Figure 7a and demonstrate that temperatures well below 500 °C are required to significantly reduce both the contribution of the BiT 00l harmonic reflections as well as the presence of the pyrochlore secondary phase.

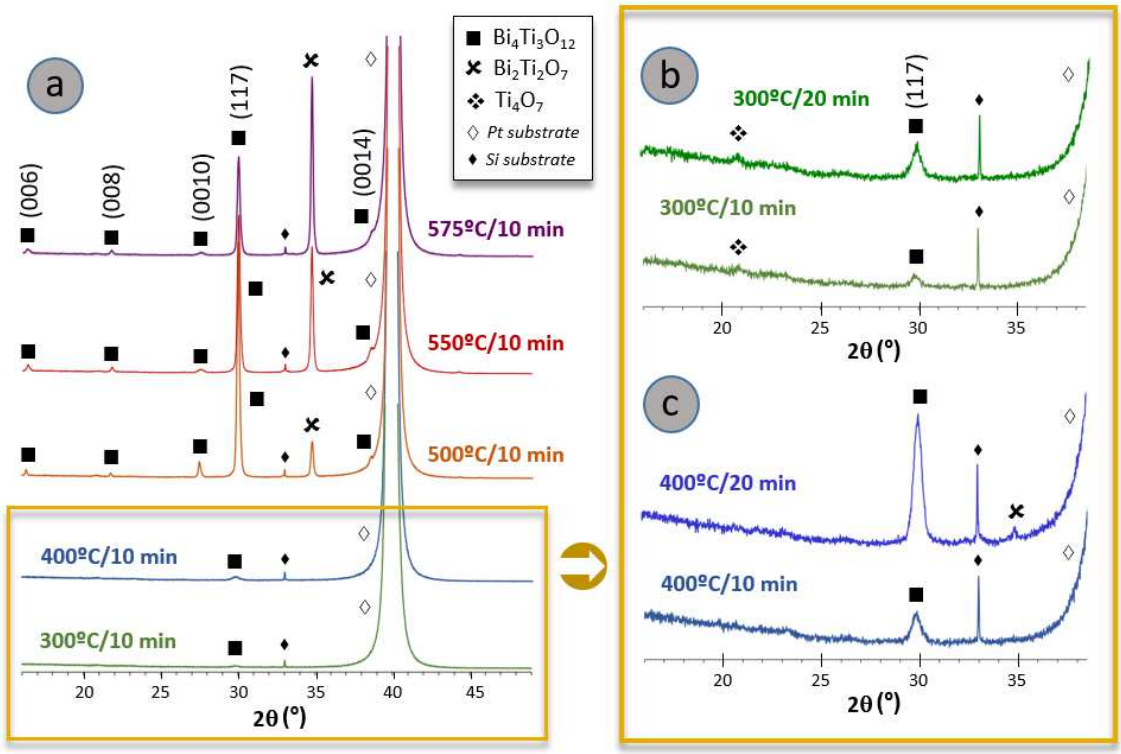



Figure 7. a) XRD patterns of the BiT films sintered at different temperatures and a dwell time of 10 minutes under solar radiation (CSE). b) CSE experiments at 300 °C. b) CSE experiments at 400 °C.

In particular, from an XRD perspective, the most promising CSE sintering conditions were achieved at 400 and 300 °C, so the dwell time was also varied for these tests, Figures 7b and 7c. This approach also brought some interesting findings. The diffractograms corresponding to the samples sintered at 300 °C first suggest that this temperature is now too low, Figure 7b. The (117) reflection of the $Bi_4Ti_3O_{12}$ phase is yet too weak and is accompanied by a small diffraction maximum that can be associated to a titanium-rich $Ti_4O_7$ intermediate phase (ICDD file no. 00-071-0574). Moreover, the persistence of this intermediate with increasing dwell time indicates a system still undergoing reaction and lacking sufficient energy input to complete the formation of the $Bi_4Ti_3O_{12}$ phase of interest. Complete phase formation appears to occur at 400 °C. At this temperature, the XRD patterns no longer show intermediate titanium phases, and the increasing crystallinity of the BIT phase with dwell time does not initially lead to (XRD) evidence of structural anisotropy, Figure 7c. Nevertheless, the CSE processing window at 400 °C also seems narrow, as the sample sintered for 20 minutes also shows incipient indications of the unwanted pyrochlore phase. All these interpretations derived from the XRD analyses were corroborated by complementary FESEM characterisation of the samples.

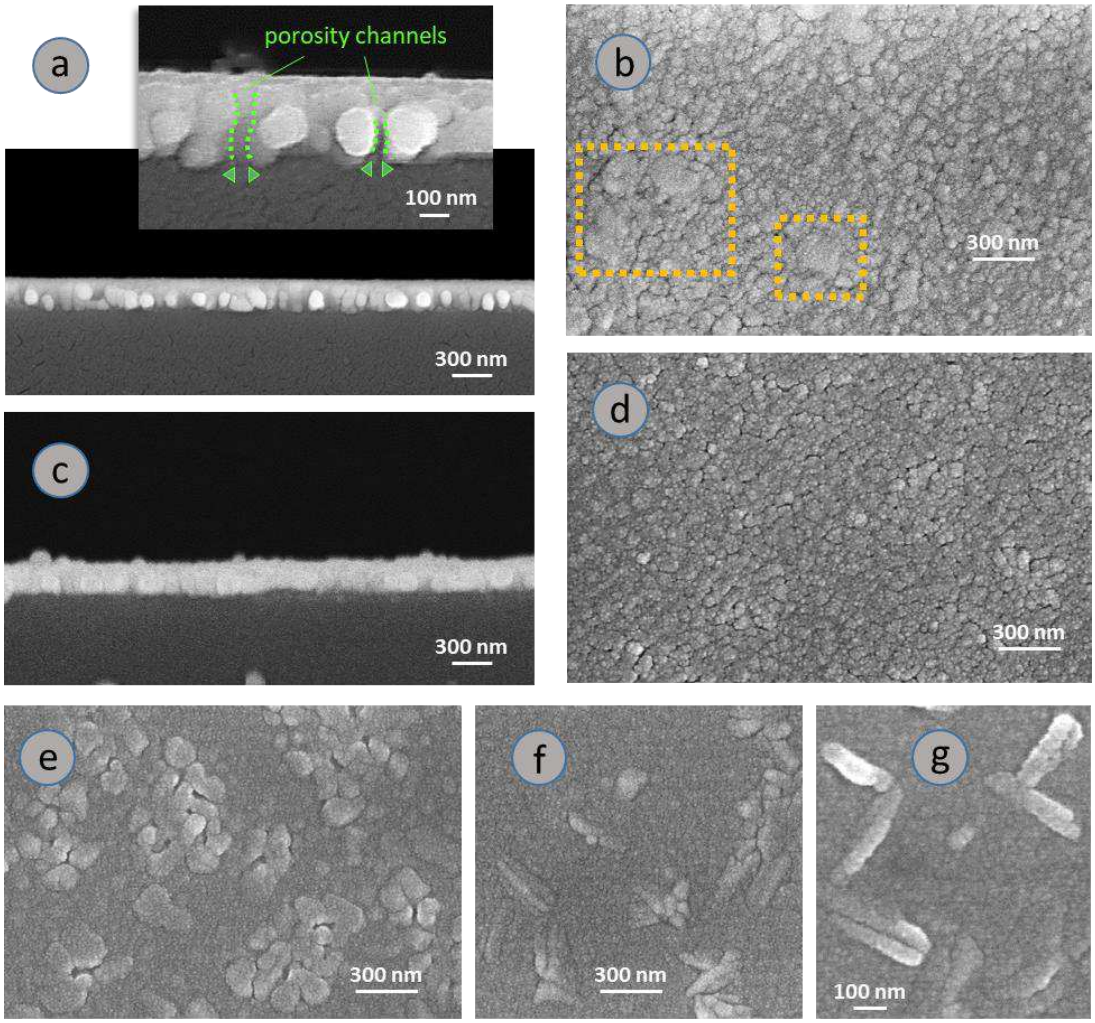



Figure 8. FESEM micrographs of the CSE BIT films obtained at a) 300 °C for 10 minutes; b) 300 °C for 20 minutes; c-b) 400 °C for 10 minutes; e-g) 400 °C for 20 minutes.

Figure 8a first shows a cross-sectional image of the film sintered by CSE at 300°C for 10 minutes, in which a uniform deposit is observed over the entire Pt/Si substrate; however, a significant lack of density is also evident, as highlighted in the enlarged image by the presence of large porosity channels between particles. The top-view micrograph in Figure 8b corresponds to the other test at 300°C (20-minute dwell time) and likewise indicates a microstructurally underdeveloped system, with regions at different stages of development (highlighted by yellow boxes), thus confirming the incomplete reaction scenario already inferred from the XRD measurements. In contrast, a homogeneous microstructure is obtained when the lens shutter is adjusted such that the film reaches a temperature of 400 °C for 10 minutes. As shown in Figures 8c and 8d, under these conditions both the density (cross-sectional image) and the microstructural homogeneity (top-view image) of the film increase substantially, while the characteristic anisotropic growth of BiT is not yet apparent. Interestingly, such anisotropic features begin to develop after an additional 10 minutes, as observed in the sample sintered at 400 °C for 20 minutes. Although the corresponding XRD patterns show no reflections associated with the (001) plane harmonics of BiT (but do indicate the onset of the pyrochlore phase, Figure 7c), the FESEM images reveal a marked evolution of the microstructure within this short time interval. This again results in some regions that are more reacted than others, Figure 8e, together with the first unequivocal signs of elongated BiT grain growth (still too small to be detected by XRD), Figures 8f and 8g. This evolution toward an anisotropic morphology represents the thermodynamic

equilibrium state of the system and defines the operational limits (processing window) of CSE conditions for achieving a non-equilibrium microstructure in BiT. Within this window, a delicate balance between kinetic acceleration and thermodynamic driving forces is established, whereby the system is sufficiently activated to achieve phase formation and densification, yet remains kinetically constrained, limiting the development of equilibrium-driven anisotropic grain growth. This provides clear evidence of the non-equilibrium nature of the solar-assisted process.

Kinetic modelling of BiT crystallisation and pyrochlore formation

To further rationalize the different crystallisation pathways observed under hot-plate and CSE treatments, a simplified kinetic analysis was introduced after the structural and microstructural characterization. The aim of this model was not to provide a complete mechanistic description of the crystallisation process, but rather to compare, in a semi-quantitative way, the relative evolution of the desired $Bi_4Ti_3O_{12}$ phase and the secondary pyrochlore phase $Bi_2Ti_2O_7$ under different thermal conditions.

The evolution of the $Bi_4Ti_3O_{12}$ phase was followed through the intensity of the (117) reflection, which corresponds to the main diffraction maximum of the orthorhombic BiT phase. In contrast, the diffraction maximum detected at approximately 35° was assigned to the $Bi_2Ti_2O_7$ pyrochlore phase, whose formation is associated with local stoichiometric deviations promoted by bismuth volatilisation during annealing. Therefore, the kinetic analysis was formulated in terms of two competing thermally activated processes: the crystallisation of the Aurivillius BiT phase and the formation of the secondary pyrochlore phase.

For each thermal treatment, the height of the selected diffraction peaks was measured and normalised with respect to the maximum value obtained for that peak within the complete experimental series. In this way, two dimensionless variables were defined: $X_{BiT}$ , associated with the (117) reflection of $Bi_4Ti_3O_{12}$, and $X_{Py}$, associated with the $Bi_2Ti_2O_7$ pyrochlore peak. Each variable ranges from 0 to 1, where 1 corresponds to the maximum relative intensity experimentally observed for that signal.

The evolution of each contribution was then approximated using a first-order thermally activated expression:

$$X_i(t) = 1 - \exp(-k_i t)$$

where $X_i$ represents diffraction signal normalised with respect to its own maximum intensity either $X_{BiT}$ or $X_{Py}$ , and $k_i$ is the corresponding apparent kinetic constant. The temperature dependence of $k_i$ was described using an Arrhenius-type relationship:

$$k_i = k_{0,i} \exp\left(-\frac{Q_i}{RT}\right)$$

where $k_{0,i}$ is the pre-exponential factor, $Q_i$ is the apparent activation energy, $R$ is the gas constant, and $T$ is the absolute temperature.

The Arrhenius analysis was retained as a semi-empirical descriptor of the competing thermally activated processes involved during annealing, as depicted in Figures 9a and 9c. Although the experimental data do not exhibit a perfectly linear Arrhenius behaviour over the complete temperature range, the model provides a useful comparative framework to evaluate the relative tendency towards $Bi_4Ti_3O_{12}$ crystallisation and pyrochlore formation under different processing conditions. Consequently, the calculated parameters

should not be interpreted as intrinsic kinetic constants, but rather as apparent kinetic descriptors associated with the overall structural evolution of the films.

For the kinetic analysis, the diffraction intensities associated with the $Bi_4Ti_3O_{12}$ (117) reflection and the pyrochlore diffraction peak were independently normalised with respect to the maximum intensity experimentally obtained for each peak within the corresponding experimental series. In this way, the resulting parameters describe the relative evolution of each crystallisation pathway with respect to its own maximum development. Therefore, the present model should be regarded as an approximate kinetic representation intended to identify general processing tendencies rather than an exact phase-fraction quantification.

This approach allows the construction of processing maps, as depicted in Figures 9b and 9d, based on the difference $\Delta X = X_{Bit} - X_{py}$. It should be interpreted as a relative kinetic dominance index rather than as an absolute difference in peak intensity or phase fraction.

This parameter was selected because both crystallisation pathways compete within the same chemical system during annealing. The formation of the Aurivillius $Bi_4Ti_3O_{12}$ phase consumes the available bismuth within the layered structure, whereas bismuth volatilisation progressively promotes local stoichiometric deviations that favour the nucleation of the $Bi_2Ti_2O_7$ pyrochlore secondary phase. Therefore, the subtraction provides an estimation of the balance between the desired crystallisation pathway and the competing degradation mechanism.

Positive values of $\Delta X$ indicate processing conditions where the $Bi_4Ti_3O_{12}$ crystallisation pathway is more developed than the pyrochlore-forming pathway, whereas values close to zero correspond to conditions where both contributions evolve similarly. Negative values, which appear mainly under concentrated solar energy processing at high temperatures and short processing times, indicate conditions where the pyrochlore contribution becomes comparatively dominant. The resulting contour maps therefore provide a qualitative representation of the processing windows in which $Bi_4Ti_3O_{12}$ crystallisation can be promoted while minimising secondary phase formation.

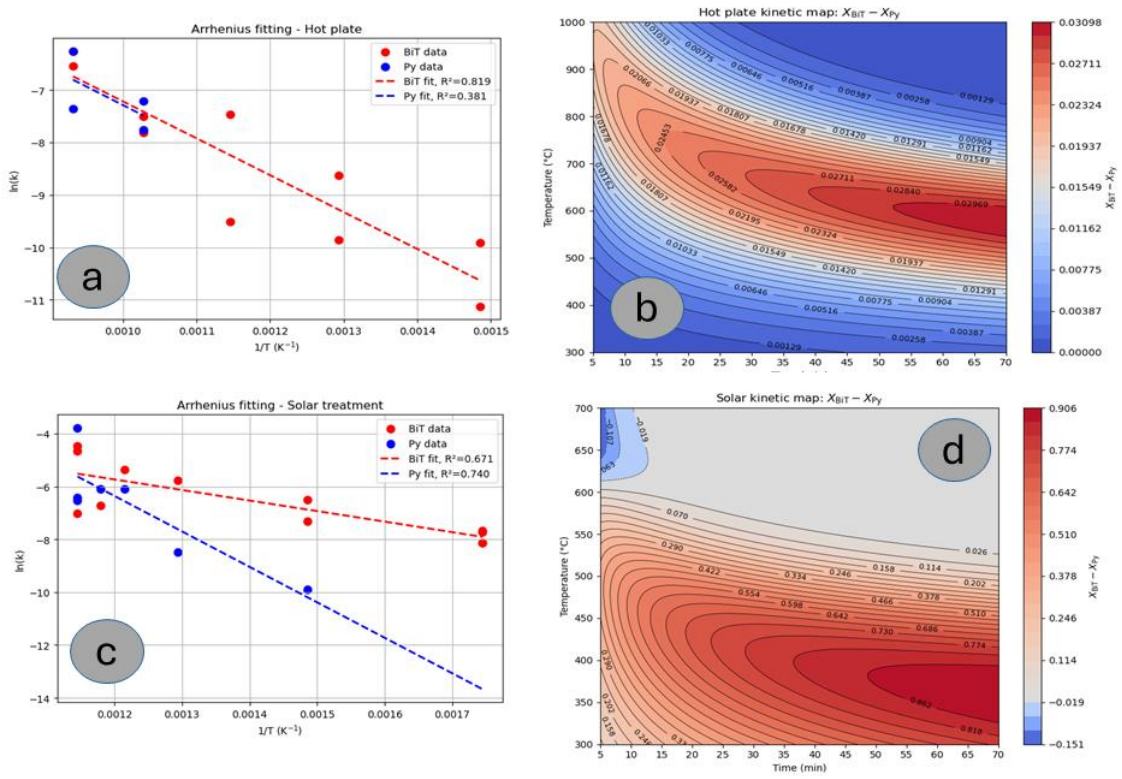



Figure 9. Semi-empirical Arrhenius fitting and kinetic dominance maps for conventional hot-plate annealing and concentrated solar energy processing. (a) Arrhenius representation for the hot-plate treatment. (b) Corresponding contour map of the kinetic dominance index ΔX. (c) Arrhenius representation for concentrated solar energy processing. (d) Corresponding contour map for the solar treatment. Positive values of ΔX indicate preferential $Bi_4Ti_3O_{12}$ crystallisation, whereas negative values indicate dominant pyrochlore formation.

## 4. Conclusions

Concentrated solar energy (CSE) has been demonstrated as an effective alternative thermal processing route for the crystallisation and sintering of $Bi_4Ti_3O_{12}$ thin films, enabling access to non-equilibrium regimes that are not attainable under conventional heating conditions. While hot-plate annealing promotes a near-equilibrium evolution of the system, leading to anisotropic grain growth and the formation of secondary phases at elevated temperatures, solar processing introduces highly localised radiative heating and rapid thermal gradients that fundamentally alter the crystallisation pathway and allow the partial decoupling of densification and grain growth. In particular, a narrow processing window around 400 °C under CSE conditions was identified, within which dense and homogeneous films can be obtained while suppressing both the development of equilibrium plate-like grains and the formation of the $Bi_2Ti_2O_7$ pyrochlore phase. At higher temperatures or long dwell times, the system rapidly evolves towards its equilibrium configuration, resulting in exaggerated anisotropic growth and enhanced bismuth volatilisation. Conversely, at lower temperatures, incomplete reaction and poor densification are observed. The demonstrated control over microstructural evolution originates from a delicate balance between kinetic acceleration and thermodynamic driving forces, underlining the strong sensitivity of CSE processing to thermal history under non-equilibrium conditions. This, combined with a significant reduction in processing times and the elimination of the need for conventional, energy-intensive heating systems, makes CSE a low-carbon and resource-efficient method for the thermal processing of functional oxide thin films. Further

studies are currently underway to determine the extent to which the functional response of $Bi_4Ti_3O_{12}$-based thin-film systems can be tailored under CSE conditions.

## Data availability

No datasets were generated or analysed during the current study.


## Acknowledgements

This work has been conducted in the frame of the research project PID2024-157669OB-I00, which was supported by the Spanish Ministry of Science, Innovation and Universities (MICIU/AEI/10.13039/501100011033) and FEDER, UE. Moreover, the authors would like to acknowledge the financial support offered by the Castilla-La Mancha Community Council, under research grant SBPLY/23/180225/000201 and co-financed by the European Regional Development Fund (ERDF).


## Compliance with ethical standards

Conflict of interest: The authors declare no competing interests.

## Author contributions

C. Gumiel: main researcher, writing original draft, M. Colado: student, methodology. D. Gomez-Lendinez: researcher, data curation, validation. A. Cañadilla: researcher, methodology. A. Romero: researcher, analysis, validation. G. P. Rodríguez: researcher, project administration, validation, supervision. A.C. Caballero: researcher, supervision. R. Barea: researcher, analysis, validation. M. Peiteado: researcher, project administration, supervision. T. Jardiel: researcher, analysis, validation, supervision

## References


[1] Arun A.P., Sreenivasan N., Patil J.H., Kusanur R., Ramachandraiah H.L., Ramakrishna M (2025) Thin films for next generation technologies: A comprehensive review of fundamentals, growth, deposition strategies, applications, and emerging frontiers. Processes 13 Article 3846. https://doi.org/10.3390/pr13123846

[2] Jayakrishna A.R., Anju B.A., Nair S.K.P., Dutta S., Silva J.P.B. (2024) Recent development of lead-free relaxor ferroelectric and antiferroelectric thin films as energy storage dielectric capacitors. J. Eur. Ceram. Soc. 44 pp. 4332-4339. https://doi.org/10.1016/j.jeurceramsoc.2024.02.016

[3] Gumiel C., Jardiel T., Villalpando A.P., Lamotte D., Calatayud D.G., Calzada M.L., Jiménez R., García-Hernández M., Mompeán F.J., Caballero A.C., Villegas M., Peiteado M. (2022) Suppressing the non-switching contribution in $BiFeO_3$-$Bi_4Ti_3O_{12}$ based thin film composites to produce room-temperature multiferroic behavior. J. Eur. Ceram. Soc. 42 pp. 5615-5623. https://doi.org/10.1016/j.jeurceramsoc.2022.06.004

[4] Vyas S. (2020) A short review on properties and applications of zinc oxide based thin films and devices. Johnson Matthey Technol. Rev. 64 pp. 202-218. https://doi.org/10.1595/205651320X15694993568524

[5] Novikov I.V., Krasnikov D.V., Lee I.H., Agafonova E.E., Serebrennikova S.I., Lee Y., Kim S., Nam J.S., Kondrashoc V.A., Han J., Rakov I.I., Nasibulin A.G. (2025) Aerosol CVD carbon nanotube thin films: From synthesis to advanced applications: A comprehensive review. Adv. Mater. 37 Article 241377. https://doi.org/10.1002/adma.202413777

[6] Catalan M.R., Malandrino G., Bongiorno C., Toro R.G., Fiorenza P., Bodeaux R., Wolfman J., Gervais M., Lambert C.A., Gervais F., Lo Nigro R. (2012) $CaCu_3Ti_4O_{12}$ thin films on conductive oxide electrode: A comparative study between chemical and physical vapor deposition routes. Mater. Chem. Phys. 133 pp. 1108-1115. https://doi.org/10.1016/j.matchemphys.2012.02.024
[7] Jolivet A., Labbé C., Frilay C., Debieu O., Marie P., Horcholle B., Lemarié F., Portier X., Grygiel C., Duprey S., Jadwisienczak W., Ingram D., Upadhyay M., David A., Fouchet A., Lüders U., Cardin J. (2023) Structural, optical, and electrical properties of $TiO_2$ thin films deposited by ALD: Impact of the substrate, the deposited thickness and the deposition temperature. Appl. Surf. Sci. 608 Article 155214. https://doi.org/10.1016/j.apsusc.2022.155214
[8] Li A., Zhu H., Guo Z., Meng Y., Liu G., Fortunato E., Martins R., Shan F. (2017) Solution combustion synthesis: Low-temperature processing for p-Type Cu:NiO thin films for transparent electronics. Adv. Mater. 29 Article 1701599. https://doi.org/10.1002/adma.201701599
[9] San-Miguel L., Castellanos-Aliaga A., Codrón R., Calatayud D.G., Caballero A., Gumiel C., Caballero A.C., Jardiel T., Peiteado M. (2025) Substrate-film interfacial interaction in the fabrication of ZnO photocatalytic thin films via sol-gel and aqueous solution-gel CSD processing. Ceram. Int. 51 pp. 46865-46878. https://doi.org/10.1016/j.ceramint.2025.07.391
[10] Grijalva-Saavedra R., Suárez-Campos G., Fuentes-Ríos J., Ruiz-Molina M., Solís-Mosquera J., Quevedo-López M.A., Cabrera-German D., Sotelo-Lerma M. (2025) Enhanced optical and electrical properties of Co-doped SnS thin films synthesized via chemical bath deposition. J. Mater. Sci. Mater. Electron. 36 Article 72. https://doi.org/10.1007/s10854-024-14126-7
[11] Jardiel T., de la Rubia M.A., Peiteado M. (2008) Control of functional microstructure in $WO_3$-doped $Bi_4Ti_3O_{12}$ ceramics. J. Am. Ceram. Soc. 91 (2008) pp 1083-1087. https://doi.org/10.1111/j.1551-2916.2008.02293.x
[12] Gumiel C., Colado M., Calatayud D.G., Barea R., Villegas M., Jardiel T. (2024) Microstructure modulation of a $Bi_4Ti_3O_{12}$ thin film system by combining the effect of a simple processing methodology with a co-doping strategy involving $Nd^{3+}$ and $Nb_{5+}$. Bol. Soc. Esp. Ceram. V. 63 pp. 425-433. https://doi.org/10.1016/j.bsecv.2024.09.002
[13] Ahn Y., Son J.Y. (2016) Mixed grains and orientation-dependent piezoelectricity of polycrystalline Nd-substituted $Bi_4Ti_3O_{12}$ thin films. Ceram. Int. 42 pp. 13061-13064. https://doi.org/10.1016/j.ceramint.2016.05.086
[14] De la Rubia M.A., Peiteado M., Fernandez J.F., Caballero A.C., Holc J., Drnovsek S., Kuscer D., Macek S., Kosec M. (2006) Thick film ZnO based varistors prepared by screen printing. J. Eur. Ceram. Soc. 26 2985-2989. https://doi.org/10.1016/j.jeurceramsoc.2006.02.016
[15] Scheld W.S., Lobe S., Dellen C., Ihrig M., Häuschen G., Hoff L.C., Finsterbusch M., Uhlenbruck S., Guillon O., Fattakhova-Rohlfing D. (2022) Rapid thermal processing of garnet-based composite cathodes. J. Power Sources 545 Article 231872. https://doi.org/10.1016/j.jpowsour.2022.231872
[16] Menon S.G., Choudhari K.S., Shivashankar S.A., Kulkarni S.D. (2025) Ten-minute synthesis of $ZnAl_2O_4$ nanoparticles by rapid annealing: dopant-induced acceleration in the crystal growth. J. Nanopart. Res. 27 Article 224. https://doi.org/10.1007/s11051-025-06423-x
[17] Ren J., Gao Y., Chen J., He Z., Deng Y., Qiu J. (2024) Effect of rapid thermal annealing treatment on up-conversion luminescence in $Er^{3+}/Yb^{3+}$ co-doped $NaYF_4$ oxy-fluoride glass-ceramics. Ceram. Int. 50 pp. 3539-3545. https://doi.org/10.1016/j.ceramint.2023.11.102
[18] Wang H. (2004) Growth and polarization feature studies on rapid thermally processed preferentially c-axis-oriented $Bi_4Ti_3O_{12}$ thin films on Si by sol-gel. Mater. Sci. Eng. B 111 pp. 64-68. https://doi.org/10.1016/j.mseb.2004.03.025
[19] Porz L., Scherer M., Huhn D., Heine L.M., Britten S., Rebohle L., Neubert M., Brown M., Lascelles P., Kitson R., Rettenwander D., Fulanovic L., Bruder E., Breckner P., Isaia D., Frömling T., Rödel J., Rheinheimer W. (2022) Blacklight sintering of ceramics. Mater. Horiz. 9 pp. 1717-1726. https://doi.org/10.1039/D2MH00177B
[20] Champagne III V.K., Pisaturo G., Clarke D.R. (2023) High temperature oxides for selective absorption of thermal radiation. J. Eur. Ceram. Soc. 43, 7656-7667. https://doi.org/10.1016/j.jeurceramsoc.2023.07.075

[21] Huang P., Yang H. (2018) A Design method to improve temperature uniformity on wafer for rapid thermal processing. Electronics 7 Article 213. https://doi.org/10.3390/electronics7100213
[22] Rosa L.G. (2019) Solar heat for materials processing: A review on recent achievements and a prospect on future trends. ChemEngineering 3 Article 83. https://doi.org/10.3390/chemengineering3040083
[23] Herranz G., Romero A., de Castro V., Rodríguez G.P. (2013) Development of high speed steel sintered using concentrated solar energy. J. Mater. Process. Technol. 213 (2013) pp. 2065-2073. https://doi.org/10.1016/j.jmatprotec.2013.06.002
[24] Fernández-González D., Ruiz-Bustinza I., González-Gasca C., Piñuela Noval J., Mochón-Castaños J., Sancho-Gorostiaga J., Verdeja L.F. (2018) Concentrated solar energy applications in materials science and metallurgy. Sol. Energy 170 pp. 520-540. https://doi.org/10.1016/j.solener.2018.05.065
[25] Romero A., Rodríguez G.P., Barea R. (2020) Sinter-hardening of chromium PM steels with concentrated solar energy. J. Mater. Process. Technol. 280 Article 116616. https://doi.org/10.1016/j.jmatprotec.2020.116616
[26] Cañadilla A., Rodríguez G.P., Romero A., Caminero M.A., Dura O.J. (2024) Sustainable production of copper components using concentrated solar energy in material extrusion additive manufacturing (MEX-CSE). Sustainable Mater. Technol. 39 Article e00799. https://doi.org/10.1016/j.susmat.2023.e00799
[27] Gonzalez-Camarillo H., Gallo A., Padilla I., Pérez-Rábago C.A., Asselineau C.A., Romero M., López-Delgado A. (2024) Design solutions and characterization of a small scale and very high concentration solar furnace using a Fresnel lens. Appl. Therm. Eng. 255 Article 124044. https://doi.org/10.1016/j.applthermaleng.2024.124044
[28] Cañadilla A., Romero A., Rodríguez G.P. (2021) Sustainable production of powder metallurgy aluminium foams sintered by concentrated solar energy. Metals 11 Article 1544. https://doi.org/10.3390/met11101544
[29] Cañadilla A., Romero A., Rodríguez G.P., Matula G., Krzemiński Ł., Tomiczek B. (2025) Manufacturing copper complex parts using an innovative Printing-Debinding-Solar Sintering (PDSS) process. J. Manuf. Processes. 134 pp. 851-865. https://doi.org/10.1016/j.jmapro.2025.01.001
[30] Romero A., Rodríguez G.P., Marjaliza E. (2022) Processing of intermetallic laminates by Self-Propagating High–Temperature Synthesis initiated with concentrated solar energy. J. Alloys Compd. 891 (2022) Article 161871. https://doi.org/10.1016/j.jallcom.2021.161876
[31] Gumiel C., Jardiel T., Calatayud D.G., Vranken T., Van Bael M.K., Hardy A., Calzada M.L., Jiménez R., García-Hernández M., Mompeán F.J., Caballero A.C., Peiteado M. (2020) Nanostructure stabilization by low-temperature dopant pinning in multiferroic $BiFeO_3$-based thin films produced by aqueous chemical solution deposition. J. Mater. Chem. C 8 pp. 4234-4245. https://doi.org/10.1039/C9TC05912A
[32] Gumiel C., Vranken T., Bernardo M.S., Jardiel T., Hardy A., Van Bael M.K., Peiteado M. (2018) Thin film composites in the $BiFeO_3$- $Bi_4Ti_3O_{12}$ system obtained by an aqueous solution-gel deposition methodology. Bol. Soc. Esp. Ceram. V. 57 pp. 19-28. https://doi.org/10.1016/j.bsecv.2017.09.001
[33] Hardy A., D´Haen J., Goux L., Wouters D., Van Bael M., Van den Rul H., Mullens J. (2007) Aqueous chemical solution deposition of ferroelectric $Ti^{4+}$ Co-substituted $(Bi,La)_4Ti_3O_{12}$ thin films. Chem. Mater. 19, 2994-3001. https://doi.org/10.1021/cm070101x
[34] Ranieri M.G.A., Aguiar E.C., Cilense M., Stojanovic B.D., Simoes A.Z., Varela J.A. (2015) Influence of processing route on electrical properties of $Bi_4Ti_3O_{12}$ ceramics obtained by tape-casting technology. Mater. Res. Bull. 70 pp. 20-25. https://doi.org/10.1016/j.materresbull.2015.03.068
[35] Jardiel T., Caballero A.C., Villegas M. (2007) Electrical properties in $WO_3$ doped $Bi_4Ti_3O_{12}$ materials. J. Eur. Ceram. Soc. 27 pp. 4115-4119. https://doi.org/10.1016/j.jeurceramsoc.2007.02.102
[36] Makovec D., Krizaj N., Meden A., Drazic G., Ursic H., Kostanjsek R., Sala M., Gyergyek S. (2022) Ferroelectric bismuth-titanate nanoplatelets and nanowires with a new crystal structure. Nanoscale 14 pp. 3537-3544. https://doi.org/10.1039/D2NR00307D
[37] Kim H., Han S.H., Kang H.W., Nahm S., Kim H.K.D., Lee J.H., Seo I. (2025) Enhancement of $BaTiO_3$ seed quality: Suppression of Bi volatilization and low-temperature synthesis in $Bi_4Ti_3O_{12}$. J. Alloys Compd. 1031 Article 181038. https://doi.org/10.1016/j.jallcom.2025.181038

[38] De la Rubia M.A., Peiteado M., de Frutos J., Rubio-Marcos F., Fernández J.F., Caballero A.C. (2007) Improved non-linear behaviour of ZnO-based varistor thick films prepared by tape casting and screen printing. J. Eur. Ceram. Soc. 27 pp. 3887-3891. https://doi.org/10.1016/j.jeurceramsoc.2007.02.057
[39] Vehkamäki M., Hatanpää T., Kemell M., Ritala M., Leskelä M. (2006) Atomic layer deposition of ferroelectric bismuth titanate $Bi_4Ti_3O_{12}$ thin films. Chem. Mater. 18 pp. 3883-3888. https://doi.org/10.1021/cm060966v
[40] Ferriere A., Rodríguez G.P., Sobrino J.A. (2004) Flux distribution delivered by a Fresnel lens used for concentrating solar energy. J. Sol. Energy Eng. 126 pp. 654-660. https://doi.org/10.1115/1.1638783